Addendum to Preliminary Hydrogeologic Characterization Results from the Wallula Basalt Pilot Study, PNWD-4129

DH Bacon
May 28, 2010

Reactive Transport Simulations

1.1 Overview

The simulations presented in section 3.2 of a previous report (McGrail et al. 2009) have been updated to include the effect of geochemical reactions between the injected CO_2 and formation minerals, and extended to longer simulation times. A description of the additional model assumptions follows in section 0, and the details of the simulation results are presented in section 0.

1.2 Geochemical Reactions

Additional simulations considered geochemical reactions involving the minerals present in the formation, the formation brine and injected supercritical CO_2. These simulations utilized the batch geochemistry solution module ECKEChem (Equilibrium-Conservation-Kinetic Equation Chemistry). This add-on module to STOMP is described in an addendum to the STOMP User's Guide (White and McGrail 2005).

ECKEChem uses an operator splitting reactive transport scheme. The operating splitting scheme solves the reactive species transport separately from the reactive species chemistry equations. The coupled nonisothermal multifluid flow and transport equations are solved sequentially with the reactive transport equations; and the reactive transport equations are solved sequentially as two components: 1) multifluid component and kinetic species transport and 2) batch chemistry. ECKEChem uses a noniterative sequential solution scheme to minimize computational costs. To reduce the number of transported species only mobile component and kinetic species are transported, which requires that transport properties, such as diffusion and dispersion coefficients are species independent. In this mathematical formulation reactive species are either components of the coupled flow and transport equations (e.g., water, air, oil, CO_2, CH_4) or dilute solutes; where, the principal assumption associated with dilute solutes is that phase properties are independent of solute concentrations. Reactive species that are components of the flow and transport equations are linked to the components via source/sink terms.

The dissolution of Columbia River Basalt under mildly acidic conditions has been assumed to be controlled by the following rate reaction:

$$r = k_{ref}\ A \exp\left[\frac{-E_a}{R}\left(\frac{1}{T}-\frac{1}{T_{ref}}\right)\right]\left(1-\frac{Q}{K_{eq}}\right)10^{(-\eta\ pH)}$$

where r is the reaction rate in mol s^{-1}, A is the surface area in m^2, k is the intrinsic rate constant in mol m^{-2} s^{-1}, E_a is the activation energy in kJ mol^{-1}, R is the universal gas constant, T is temperature in degrees

Kelvin, and η is the pH power law coefficient. The mineral composition of the basalt (Table 1), rate parameters for the primary constituents of the basalt (Table 2), and secondary minerals that may precipitate after injection of CO_2 (Table 3) are taken from laboratory experiments on Columbia River Basalt (Schaef et al. In Press) and related batch chemistry simulations using EQ3/6 (Wolery and Jarek 2003). Kinetic data for secondary minerals were taken from published rates (Palandri and Kharaka 2004; Xu et al. 2005). Pertinent equilibrium aqueous reactions and their equilibrium coefficients were determined using the EQ3/6 version 8.0 COMP database (Wolery and Jarek 2003).

Initial conditions for aqueous species concentrations were based on groundwater sampling, detailed in Appendix A of PNWD-4129, from test zone 8B. Total initial aqueous concentrations for each element are shown in Table 5.

Table 1. Mineral Composition of Basalt

Mineral	Volume Fraction	Specific Gravity, g cm^{-3}
Plagioclase	0.374	2.69
Clinopyroxene	0.191	3.37
Mesostasis	0.425	2.65
Magnetite	0.011	5.2

Table 2. Primary Mineral Kinetic Reactions

Reaction	log K_{eq}	k_{ref} at T_{ref}, mol m^{-2} s^{-1}	T_{ref}, °C	E_a, kJ mol^{-1}	η
Plagioclase + $6.186H^+ = 1.5465\ Al^{+++} + 0.4535Na^+ + 3.093H_2O + 2.4535SiO_2 + 0.5465Ca^{++}$	15.29	8.03×10^{-08}	60	42.1	0.626
Clinopyroxene + $4H^+ = Ca^{2+} + 0.25Fe^{2+} + 0.75Mg^{2+} + 2H_2O + 2SiO_2(aq)$	19.89	4.13×10^{-06}	60	78.0	0.700
Mesostasis + $0.8869H^+ = 0.429H_2O + 0.2051Al^{+++} + 0.0378Ca^{2+} + 0.0364Fe^{2+} + 0.0329K^+ + 0.0049Mg^{2+} + 0.0056Mn^{2+} + 0.0693Na^+ + SiO_2(aq) + 0.007Ti(OH)4(aq)$	-2.60	3.93×10^{-08}	100	30.3	0.318
Magnetite + $6H^+ = 3Fe^{2+} + 0.5O_2(g) + 3H_2O$	-5.15	8.34×10^{-11}	60	18.6	0.279

Table 3. Secondary Mineral Kinetic Reactions

Reaction	log K_{eq}	k_{ref} at T_{ref}, mol m^{-2} s^{-1}	T_{ref}, °C	E_a, kJ mol^{-1}	η
Anatase $+2H_2O = Ti(OH)_4(aq)$	-9.65	4.47×10^{-09}	25	37.9	0.421
Beidellite-Ca + $7.32H^+ + = 0.165Ca^{2+} + 2.33Al^{3+} + 3.67SiO_2(aq)$	4.65	1.05×10^{-11}	25	23.6	0.340
Beidellite-K + $7.32H^+ + = 0.33K^+ + 2.33Al^{3+} + 3.67SiO_2(aq)$	4.43	1.05×10^{-11}	25	23.6	0.340
Beidellite-Mg + $7.32H^+ + = 0.165Mg^{2+} + 2.33Al^{3+} + 3.67SiO_2(aq)$	4.60	1.05×10^{-11}	25	23.6	0.340

Calcite + $H^+ = Ca^{2+} + HCO_3^-$	1.70	5.01×10^{-01}	25	14.4	1.000
Chalcedony = $SiO_2(aq)$	-3.56	5.89×10^{-13}	25	74.5	0.000
Dawsonite + $3H^+ = Al^{3+} + Na^+ + HCO_3^-$	3.91	1.00×10^{-07}	25	62.8	0.000
Dolomite + $2H^+ = Ca^{2+} + Mg^{++} + 2HCO_3^-$	2.17	1.74×10^{-04}	25	56.7	0.500
Rhodochrosite + $H^+ = HCO_3^- + Mn^{2+}$	-0.32	1.02×10^{-03}	25	21.0	0.900
Siderite + $H^+ = Fe^{2+} + HCO_3^-$	-0.38	1.02×10^{-03}	25	21.0	0.900

Table 4. Equilibrium Aqueous Reactions

Reaction	log K
$OH^- + H^+ = H_2O$	-13.681
$Al(OH)_2^+ + 2H^+ = Al^{3+} + 2H_2O$	-10.032
$AlO_2^- + 4H^+ = Al^{3+} + 2H_2O$	-21.854
$AlOH^{2+} + H^+ = Al^{3+} + H_2O$	-4.671
$HCO_3^- + H^+ = CO_2(aq) + H_2O$	-6.297
$CO_3^{2-} + 2H^+ = CO_2(aq) + H_2O$	-16.547
$CaCO_3(aq) + 2H^+ = CO_2(aq) + Ca^{2+} + H_2O$	-13.126
$CaHCO3+ + H^+ = CO_2(aq) + Ca^{2+} + H_2O$	-5.236
$Fe(OH)_3(aq) + 2H^+ = Fe^{2+} + 0.25O_2(aq) + 2.5H_2O$	-4.807
$Fe(OH)_4^- + 3H^+ = Fe^{2+} + 0.25O_2(aq) + 3.5H_2O$	-14.407
$FeHCO_3^+ + H^+ = CO_2(aq) + Fe^{2+} + H_2O$	-3.577
$HAlO_2(aq) + 3H^+ = Al^{3+} + 2H_2O$	-15.606
$HSiO_3^- + H^+ = + SiO_2(aq) + H_2O$	-9.807
$MgCO_3(aq) + 2H^+ = CO_2(aq) + Mg^{++} + H_2O$	-13.513
$MgHCO_3^+ + H^+ = CO_2(aq) + Mg^{++} + H_2O$	-5.243
$MnCO_3(aq) + 2H^+ = CO_2(aq) + Mn^{++} + H_2O$	-12.106
$MnHCO_3^+ + H^+ = CO_2(aq) + Mn^{2+} + H_2O$	-5.415
$MnOH^+ + H^+ = Mn^{2+} + H_2O$	-10.59
$NaHCO_3(aq) + H^+ = CO_2(aq) + Na^+ + H_2O$	-6.222
$NaHSiO_3(aq) + H^+ = Na^+ + SiO_2(aq) + H_2O$	-8.238
$OH^- + H^+ = H_2O$	-13.681
$Al(OH)_2^+ + 2H^+ = Al^{3+} + 2H_2O$	-10.032
$AlO_2^- + 4H^+ = Al^{3+} + 2H_2O$	-21.854
$AlOH^{2+} + H^+ = Al^{3+} + H_2O$	-4.671

Table 5. Initial Aqueous Concentrations

Element	Concentration, mol/L
Al	8.48×10^{-6}
Ca	2.70×10^{-5}
Fe	1.72×10^{-5}
K	6.01×10^{-5}
Mg	4.53×10^{-6}
Mn	2.57×10^{-7}
Na	4.03×10^{-3}
Si	1.28×10^{-3}
Ti	2.26×10^{-10}
pH	9.68

1.3 Results

The total mass of CO_2 modeled for the injection simulations was 1000 metric tons (MT), which was injected over a time period of either 14 or 30 days. For possible pilot study design considerations, three different injection scenarios were considered:

- Scenario 1: simultaneous injection into the OFT, SCFT1 and SCFT2 over a period of 14 days,
- Scenario 2: injection into only the SCFT2 over a period of 14 days, and
- Scenario 3: injection into only the OFT over a period of 30 days.

1.3.1 Scenario 1: Injection into OFT, SCFT1 and SCFT2

The radius of the injected supercritical CO_2 from the Wallula pilot borehole well increases from 70 ft after the active 2 weeks of injection into OFT, SCFT1 and SCFT2 to 200 ft at 6 years after the start of injection (Figure 1). At 13 years after the start of injection the radius begins to decrease.

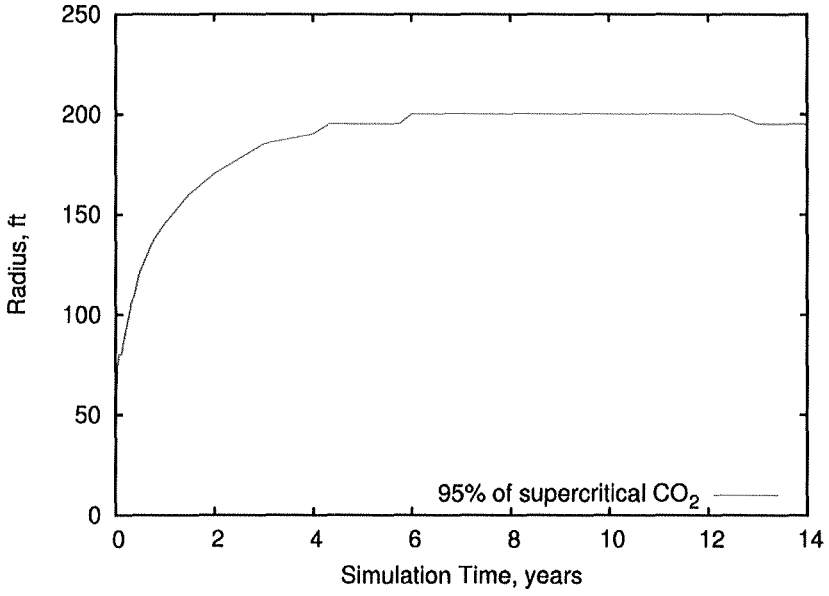

Figure 1. Radii Containing 95% of 1000 MT of Supercritical CO_2 Injected into the Ortley, Slack Canyon #1 and Slack Canyon #2 Flow Tops

More of the injected CO_2 flows into the SCFT2 (Figure 2); this zonal preferential injection of CO_2 is a result of the higher permeability exhibited by SCFT2.

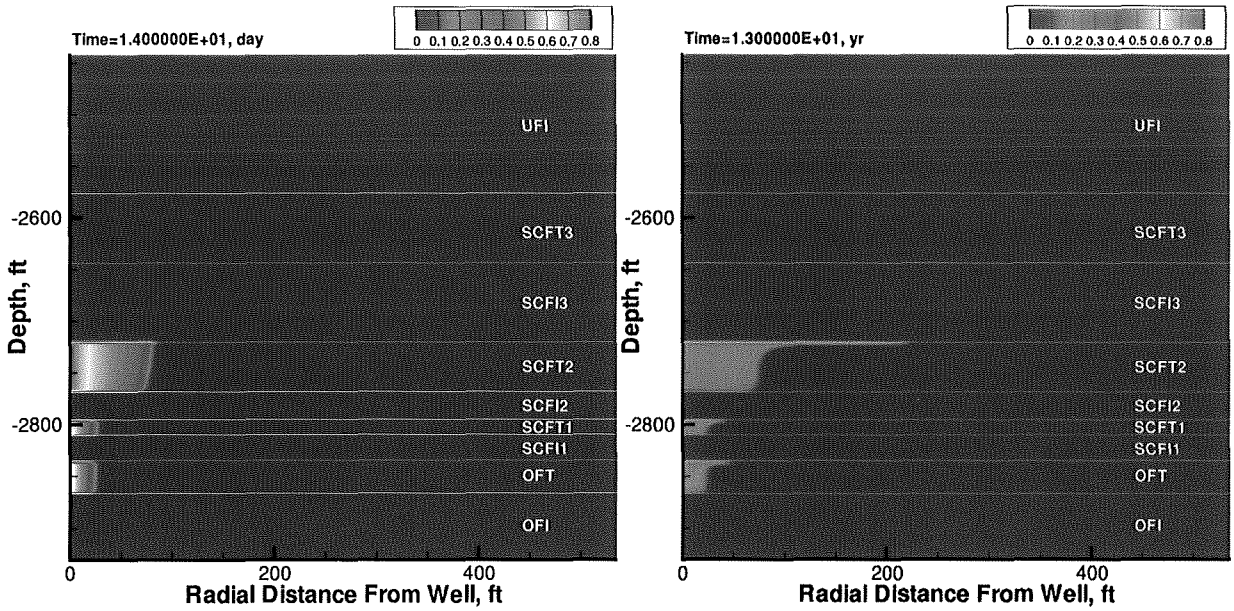

Figure 2. CO_2 Saturation (a) 14 days and (b) 13 years after 1000 MT Supercritical CO_2 Injection into the Ortley, Slack Canyon #1 and Slack Canyon #2 Flow Tops

After the injection of supercritical CO_2, CO_2 dissolves into the aqueous phase, up to the equilibrium solubility limit. Aqueous CO_2 dissociates into bicarbonate and carbonate ions, producing H^+ and lowering the pH. The pH of the residual formation water in contact with the injected CO_2 decreases from an initial value of 9.6 to values as low as 4 just after injection. Over the 13-year recovery period, the pH increases slightly to an average value of 4.9 (Figure 3). The lowered pH drives the dissolution of primary minerals in the basalt, producing Ca^+, Mg^+ and Fe^+ which combine with the aqueous CO_2 to form carbonate secondary minerals. Over time, as the injected CO_2 spreads, allowing more CO_2 to dissolve; the total amount of supercritical CO_2 decreases and amounts of dissolved and mineral CO_2 increase (Figure 4). After 13 years, 24.8% of the injected CO_2 has dissolved and 24.8% has precipitated as carbonate minerals.

The glassy mesostasis dissolves most rapidly (Figure 5) which drives the precipitation of several secondary minerals (Figure 6). In the vicinity of the injected CO_2, the most prevalent secondary carbonate minerals are dolomite (Figure 7) and calcite (Figure 8). After 3 years, porosity changes in the formation are slight, less than 1.86% decrease near the upper and lower edges of the injected CO_2 at the caprock boundaries (Figure 9).

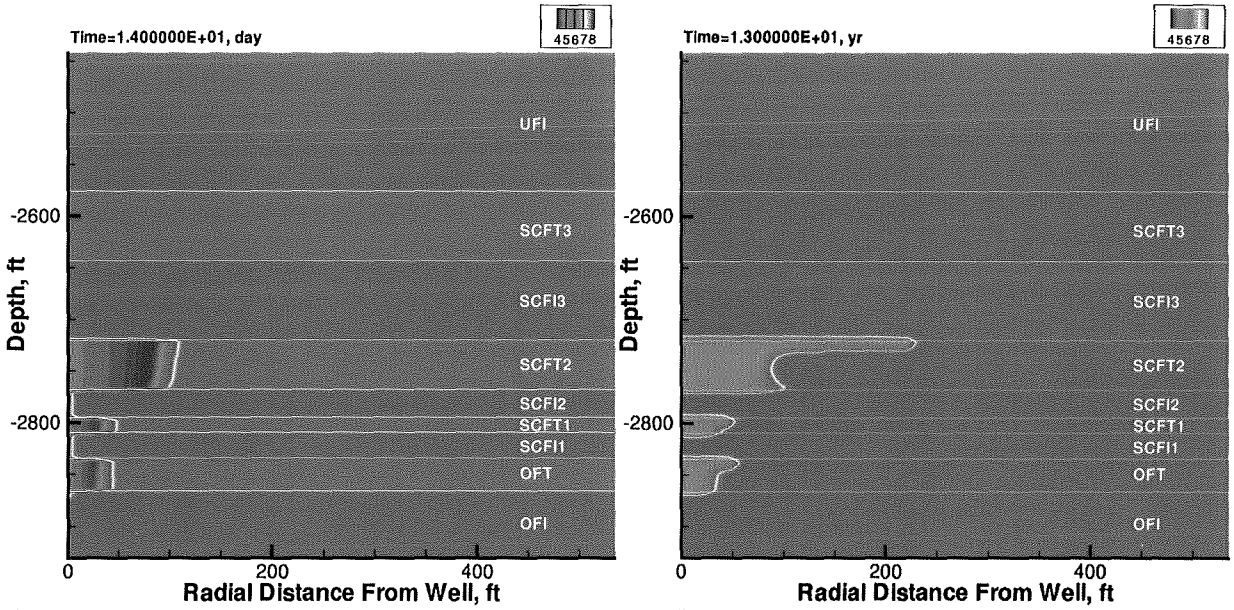

Figure 3. Distribution of pH after (a) 14 days and (b) 13 years after 1000 MT Supercritical CO_2 Injection into the Ortley, Slack Canyon #1 and Slack Canyon #2 Flow Tops. Ambient pH is 9.6.

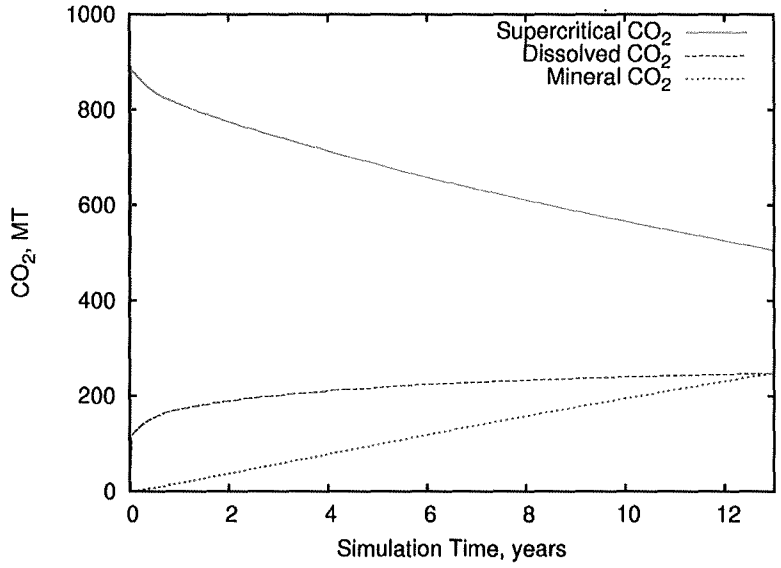

Figure 4. Mass balance of 1000 MT of CO_2 Injection into the Ortley, Slack Canyon #1 and Slack Canyon #2 Flow Tops.

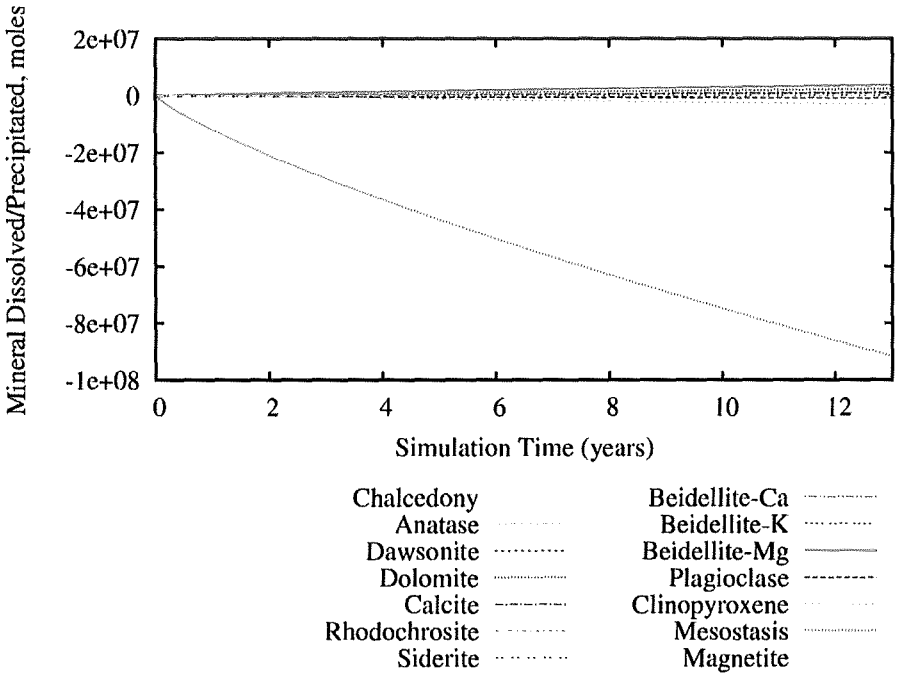

Figure 5. Change in mineral mass (total moles in model domain, negative value indicates dissolution, positive value indicates precipitation) after 1000 MT of CO_2 Injection into the Ortley, Slack Canyon #1 and Slack Canyon #2 Flow Tops.

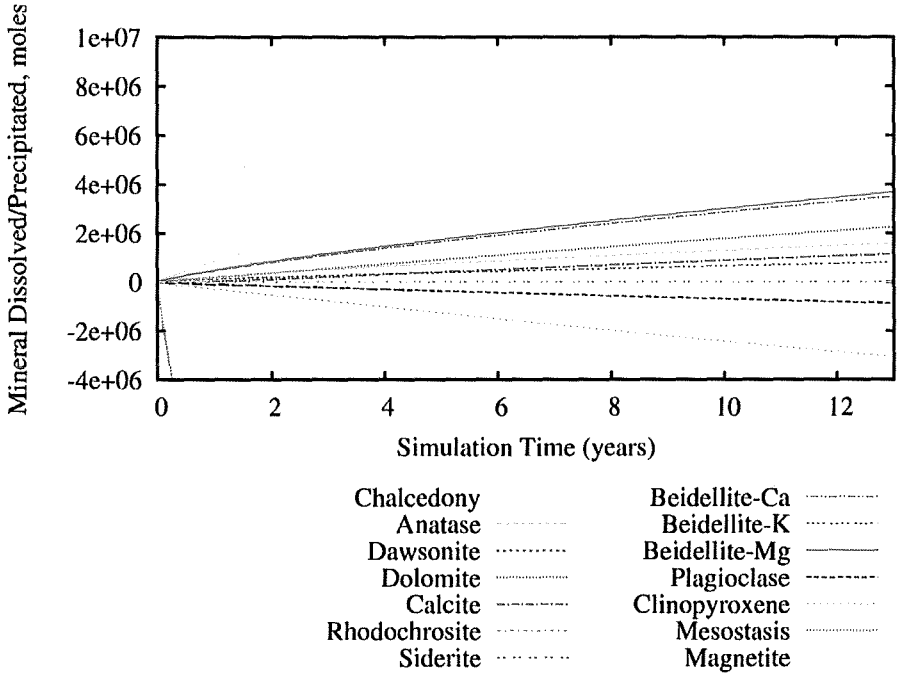

Figure 6. Closeup of Figure 5 showing detail of minerals other than mesostasis (total moles in model domain).

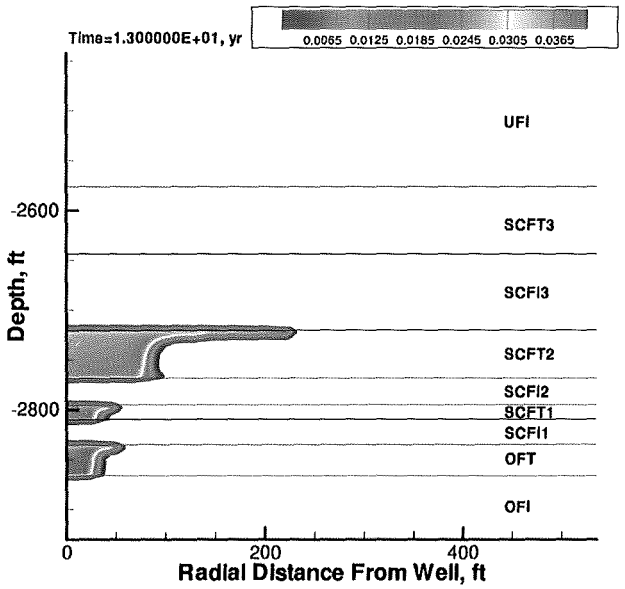

Figure 7. Distribution of precipitated dolomite (moles m^{-3}) 13 years after 1000 MT of CO_2 Injection into the Ortley, Slack Canyon #1 and Slack Canyon #2 Flow Tops.

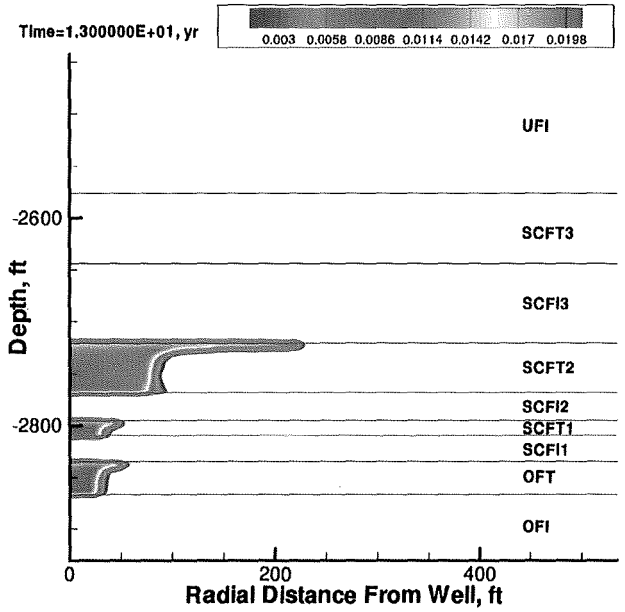

Figure 8. Distribution of precipitated calcite (moles m^{-3}) 13 years after 1000 MT of CO_2 Injection into the Ortley, Slack Canyon #1 and Slack Canyon #2 Flow Tops.

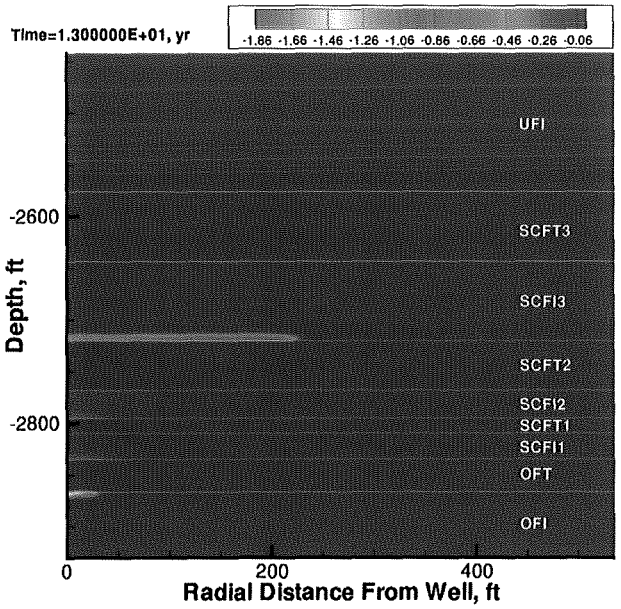

Figure 9. Porosity change (%) in formation 13 years after 1000 MT of CO_2 Injection into the Ortley, Slack Canyon #1 and Slack Canyon #2 Flow Tops.

The density of the injected supercritical CO_2 is 60% of that exhibited by groundwater at the prevailing formation temperature and pressure conditions. Because supercritical CO_2 does not displace all of the groundwater within the formation pore space, and a significant amount of the supercritical CO_2 has dissolved or precipitated, the average fluid-density contrast is 75% to 100% of that exhibited by the initial formation water after 14 days (Figure 10a) and 90% to 100% that of initial formation water after 13 years (Figure 10b).

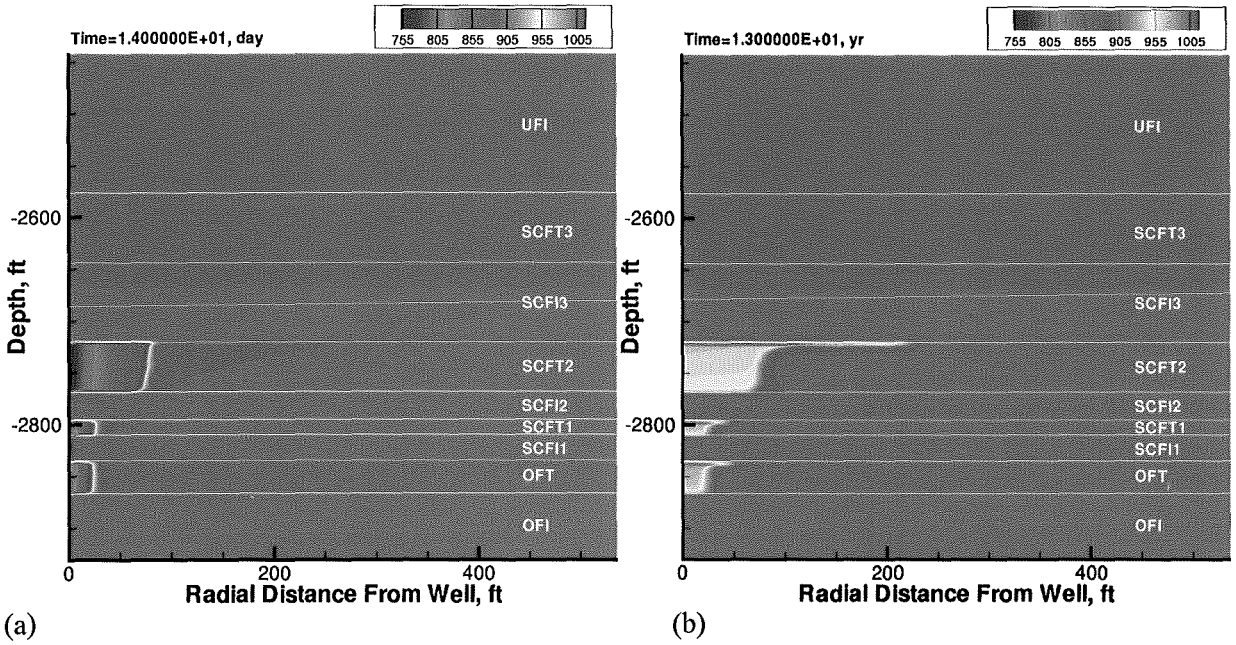

Figure 10. Fluid Density (kg/m^3) in the Ortley, Slack Canyon #1, and Slack Canyon #2 Flow Tops (a) 14 days and (b) 13 years after start of 1000 MT Supercritical CO_2 Injection

1.3.1.1 Scenario 2: Injection into Slack Canyon #2 Flow Top (SCFT2)

The radius of the injected supercritical CO_2 from the Wallula pilot borehole well increases from 75 ft after the active 2 weeks of injection into SCFT2 to 210 ft at 6.25 years after the start of injection (Figure 11). At 13 years after the start of injection the radius begins to decrease.

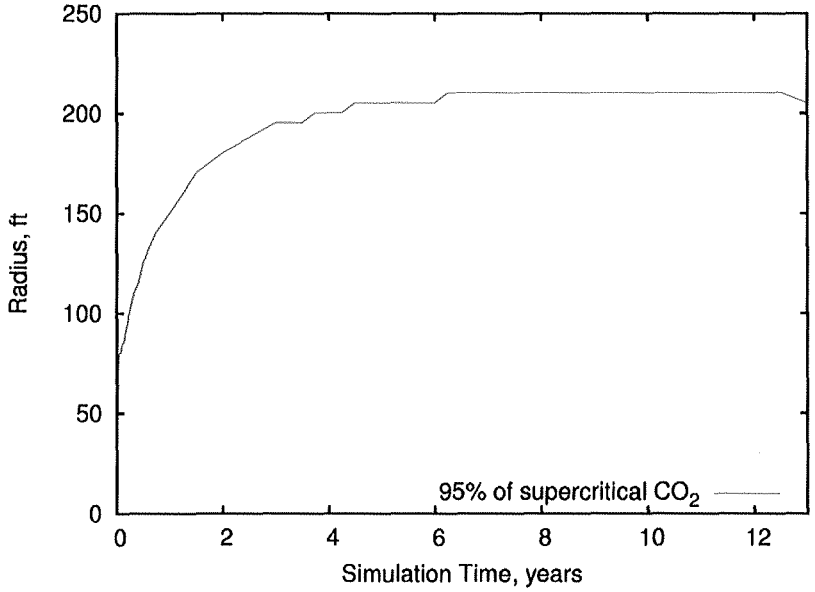

Figure 11. Radii Containing 95% of 1000 MT of Supercritical CO_2 Injected into the Slack Canyon #2 Flow Top

Because most of the CO_2 injected in the previous Scenario 1 ended up in the SCFT2, a simulation assuming all CO_2 is injected directly into the SCFT2 does not produce significantly different results (Figure 12).

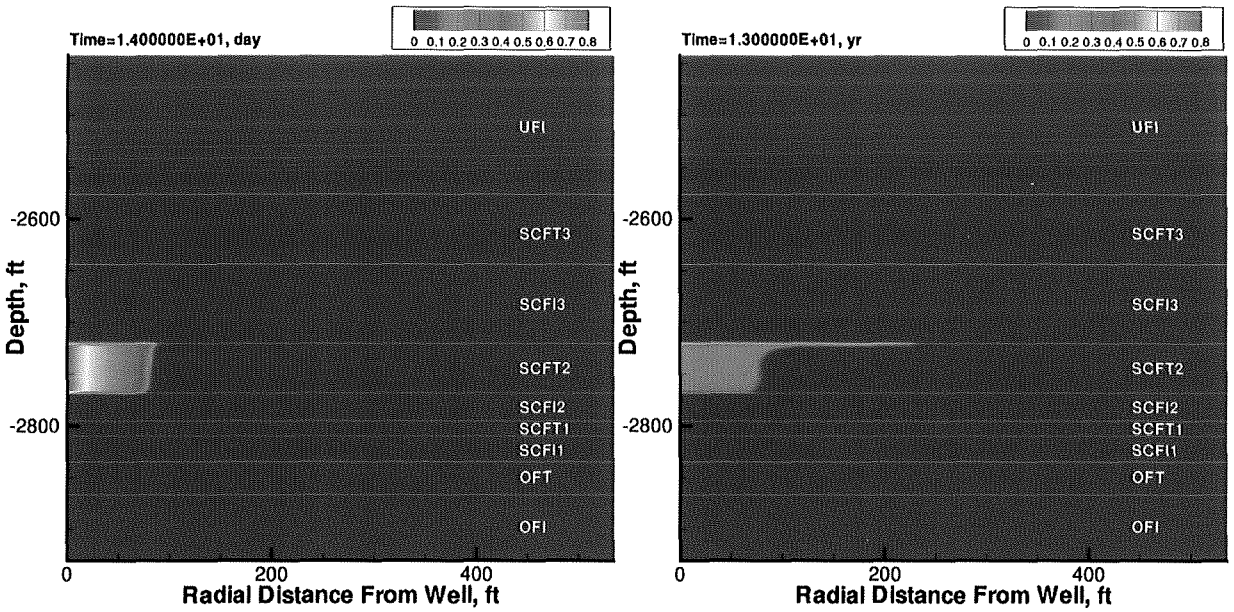

Figure 12. CO_2 Saturation (a) 14 days and (b) 13 years after 1000 MT Supercritical CO_2 Injection into the Slack Canyon #2 Flow Top

After the injection of supercritical CO_2, CO_2 dissolves into the aqueous phase, up to the equilibrium solubility limit. Aqueous CO_2 dissociates into bicarbonate and carbonate ions, producing H^+ and lowering the pH. The pH of the residual formation water in contact with the injected CO_2 decreases from an initial value of 9.6 to values as low as 4 just after injection. Over the 13-year recovery period, the pH increases slightly to an average value of 4.9 (Figure 13). The lowered pH drives the dissolution of primary minerals in the basalt, producing Ca^+, Mg^+ and Fe^+ which combine with the aqueous CO_2 to form carbonate secondary minerals. Over time, as the injected CO_2 spreads, allowing more CO_2 to dissolve; the total amount of supercritical CO_2 decreases and amounts of dissolved and mineral CO_2 increase (Figure 14). After 13 years, 24.6% of the injected CO_2 has dissolved and 24.4% has precipitated as carbonate minerals.

The glassy mesostasis dissolves most rapidly (Figure 15) which drives the precipitation of several secondary minerals (Figure 16). In the vicinity of the injected CO_2, the most prevalent secondary carbonate minerals are dolomite (Figure 17) and calcite (Figure 18). After 3 years, porosity changes in the formation are slight, less than 1.15% decrease near the upper and lower edges of the injected CO_2 at the caprock boundaries (Figure 19).

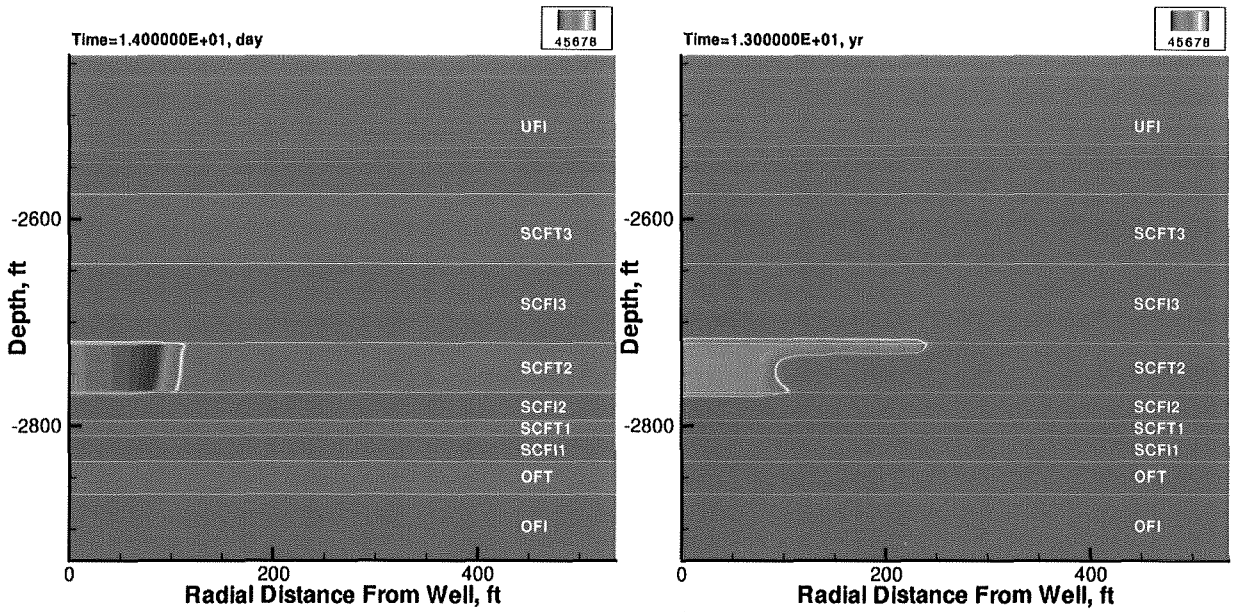

Figure 13. Distribution of pH after (a) 14 days and (b) 13 years after 1000 MT Supercritical CO_2 Injection into the Slack Canyon #2 Flow Top. Ambient pH is 9.6.

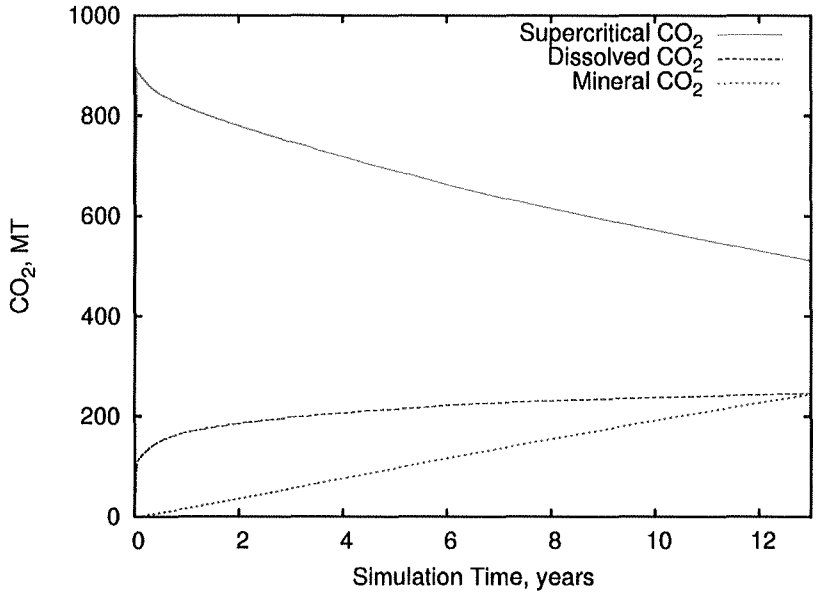

Figure 14. Mass balance of 1000 MT of CO_2 Injection into the Slack Canyon #2 Flow Top.

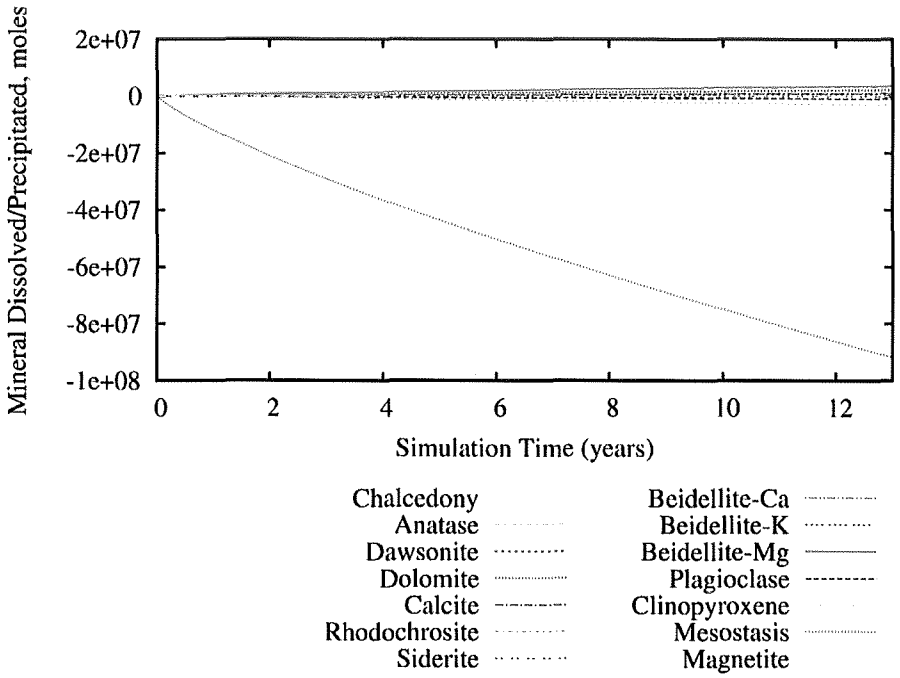

Figure 15. Change in mineral mass (total moles in model domain, negative value indicates dissolution, positive value indicates precipitation) after 1000 MT of CO_2 Injection into the Slack Canyon #2 Flow Top.

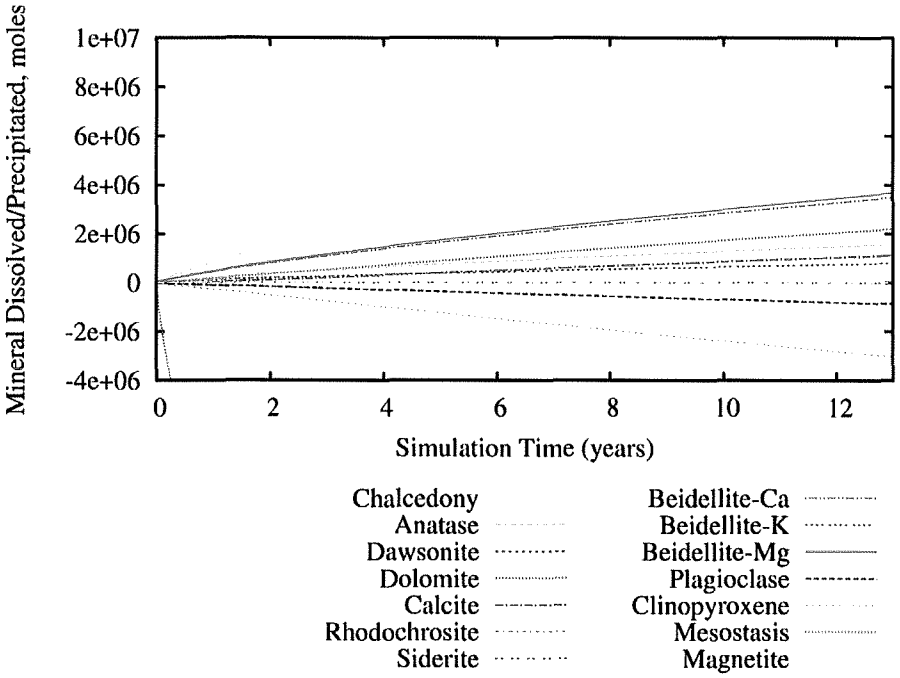

Figure 16. Closeup of Figure 15 showing detail of minerals other than mesostasis (total moles in model domain).

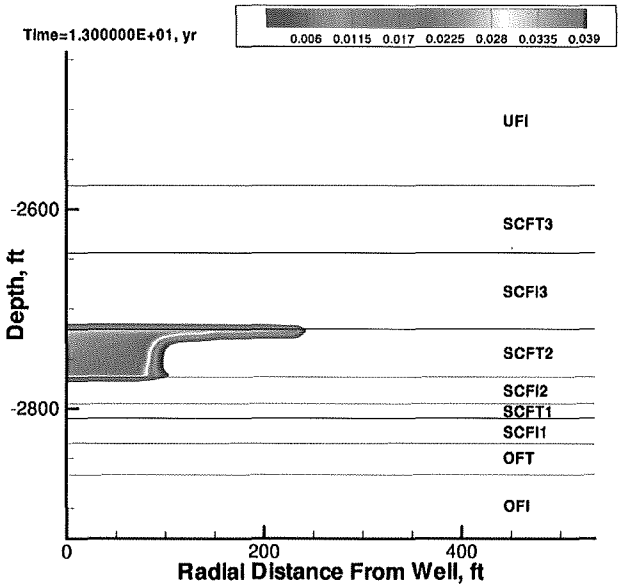

Figure 17. Distribution of precipitated dolomite (moles m^{-3}) 13 years after 1000 MT of CO_2 Injection into the Slack Canyon #2 Flow Top.

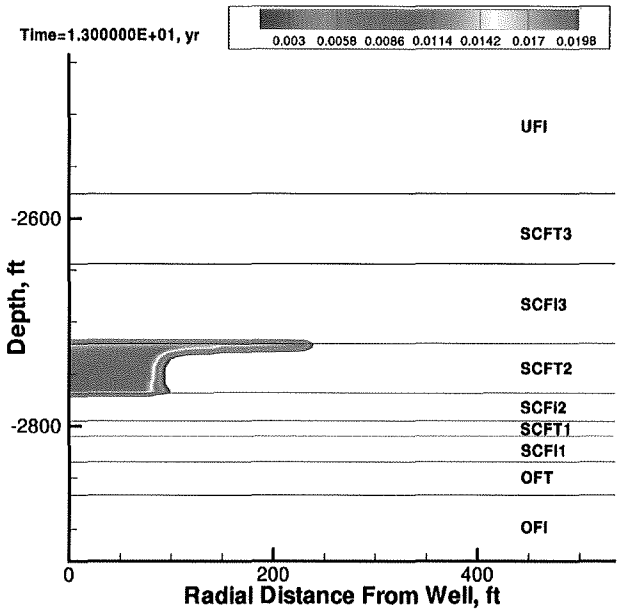

Figure 18. Distribution of precipitated calcite (moles m^{-3}) 13 years after 1000 MT of CO_2 Injection into the Slack Canyon #2 Flow Top.

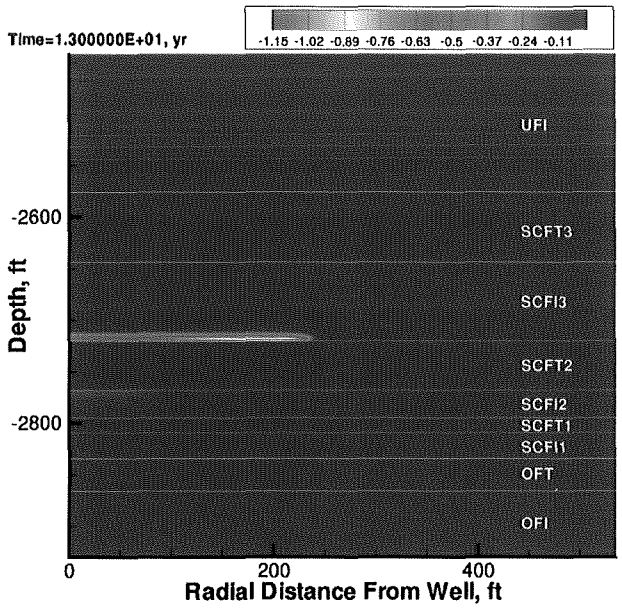

Figure 19. Porosity change (%) in formation 13 years after 1000 MT of CO_2 Injection into the Slack Canyon #2 Flow Top.

The density of the injected supercritical CO_2 is 60% of that exhibited by groundwater at the prevailing formation temperature and pressure conditions. Because supercritical CO_2 does not displace all of the groundwater within the formation pore space, and a significant amount of the supercritical CO_2 has dissolved or precipitated, the average fluid-density contrast is 75% to 100% of that exhibited by the initial formation water after 14 days (Figure 20a) and 90% to 100% that of initial formation water after 13 years (Figure 20b).

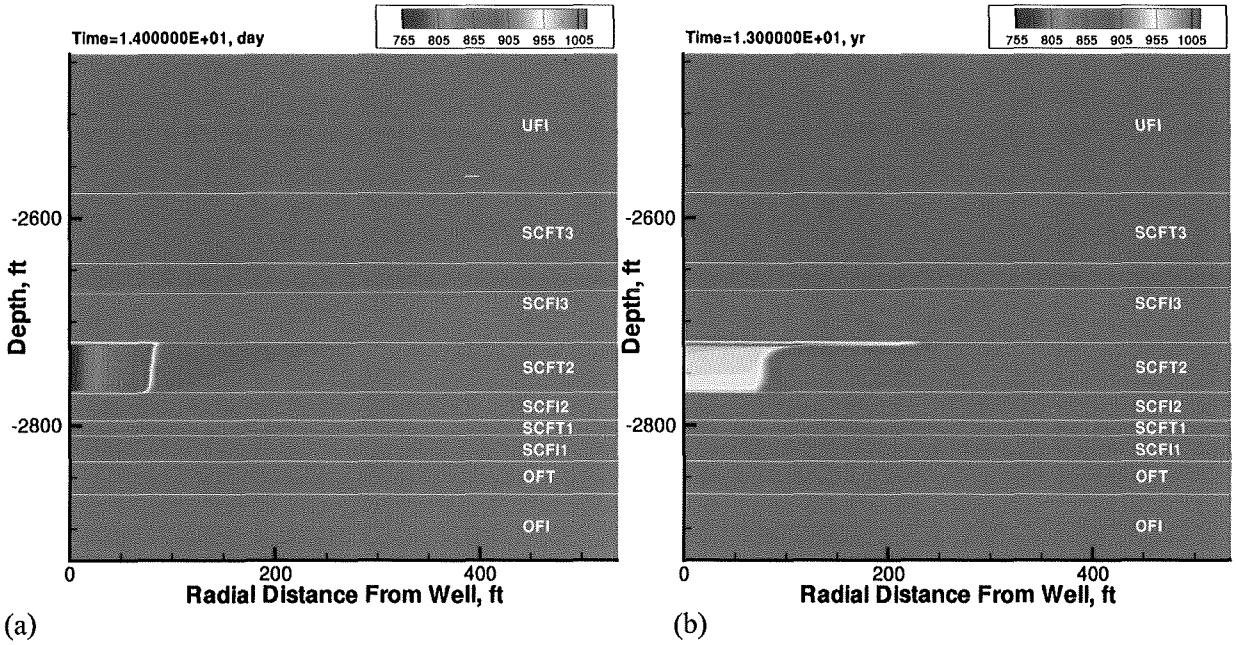

Figure 20. Fluid Density (kg/m^3) in the Slack Canyon #2 Flow Top (a) 14 days and (b) 13 years after start of 1000 MT Supercritical CO_2 Injection

1.3.1.2 Scenario 3: Injection into Ortley Flow Top (OFT)

The radius of the injected supercritical CO_2 from the Wallula pilot borehole well increases from 90 ft after the active 30 days of injection into OFT to 170 ft at 18 years after the start of injection (Figure 21). At 37 years after the start of injection the radius begins to decrease. The lower permeability of the OFT results in a longer time for the plume to stop spreading.

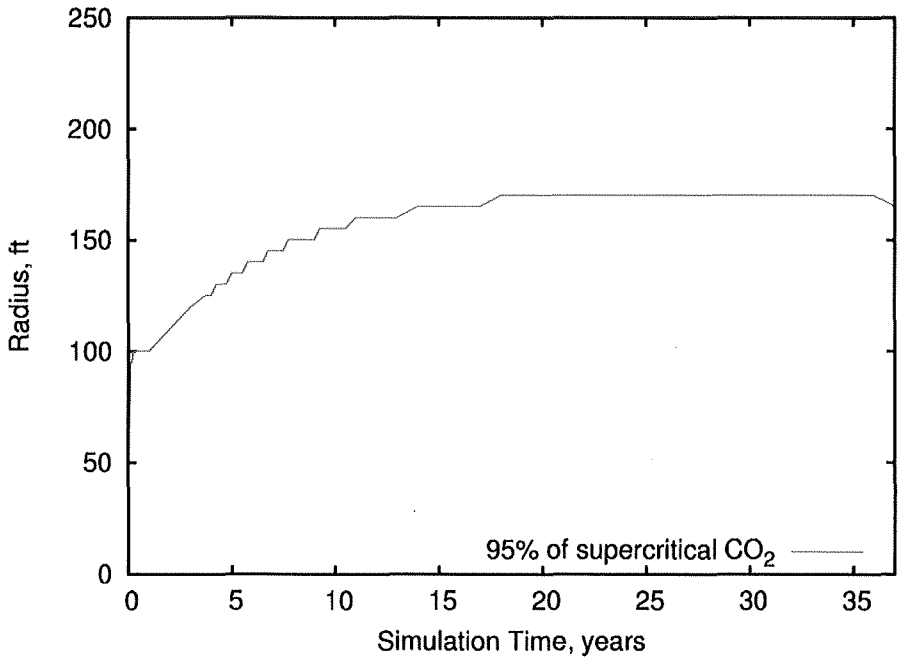

Figure 21. Radii Containing 95% of 1000 MT of Supercritical CO_2 Injected into the Ortley Flow Top

Although the OFT is thinner than the SCFT2 with identical porosity, the lower permeability of the OFT results in a more compact CO_2 plume (Figure 22).

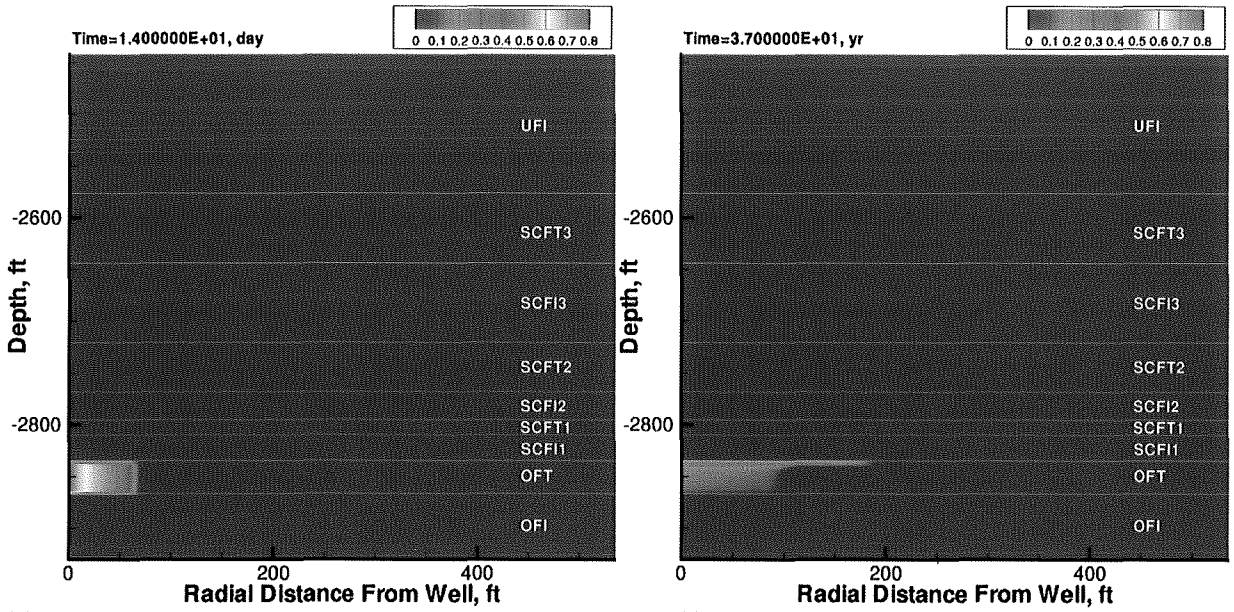

Figure 22. CO_2 Saturation (a) 14 days and (b) 37 years after 1000 MT Supercritical CO_2 Injection into the Ortley Flow Top

After the injection of supercritical CO_2, CO_2 dissolves into the aqueous phase, up to the equilibrium solubility limit. Aqueous CO_2 dissociates into bicarbonate and carbonate ions, producing H^+ and lowering the pH. The pH of the residual formation water in contact with the injected CO_2 decreases from an initial value of 9.6 to values as low as 4 just after injection. Over the 37-year recovery period, the pH increases slightly to an average value of 4.9 (Figure 23). The lowered pH drives the dissolution of primary minerals in the basalt, producing Ca^+, Mg^+ and Fe^+ which combine with the aqueous CO_2 to form carbonate secondary minerals. Over time, as the injected CO_2 spreads, allowing more CO_2 to dissolve; the total amount of supercritical CO_2 decreases and amounts of dissolved and mineral CO_2 increase (Figure 24). After 37 years, 18.9% of the injected CO_2 has dissolved and 44.3% has precipitated as carbonate minerals.

The glassy mesostasis dissolves most rapidly (Figure 25) which drives the precipitation of several secondary minerals (Figure 26). In the vicinity of the injected CO_2, the most prevalent secondary carbonate minerals are dolomite (Figure 27) and calcite (Figure 28). After 3 years, porosity changes in the formation are small, less than 2.18% decrease near the upper and lower edges of the injected CO_2 at the caprock boundaries (Figure 29).

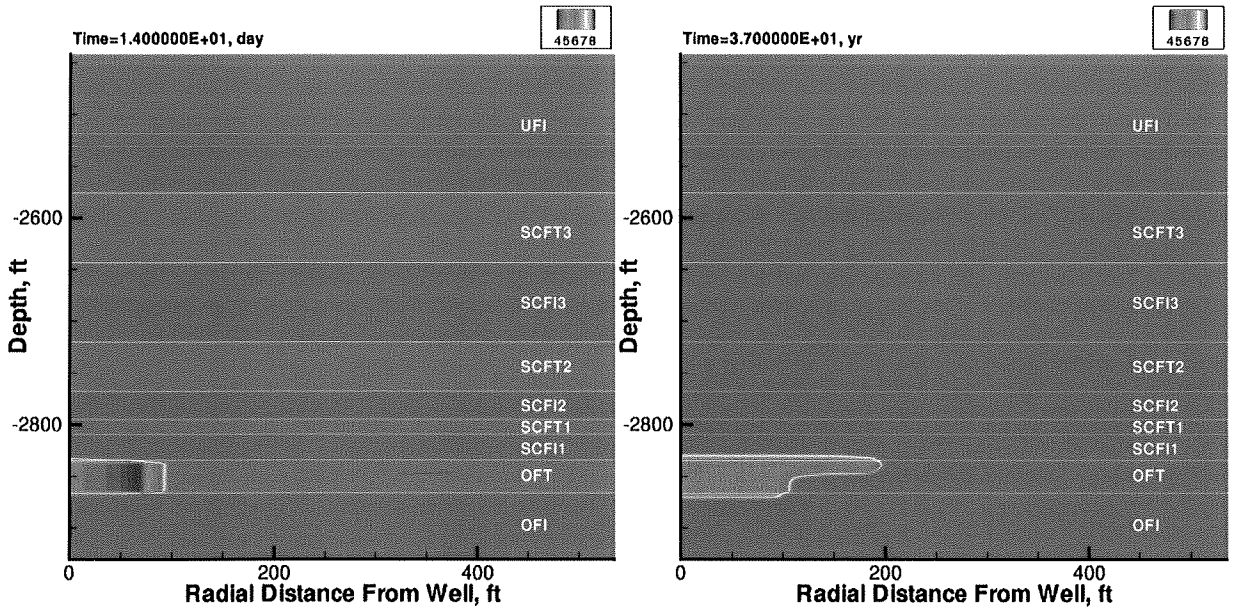

Figure 23. Distribution of pH after (a) 14 days and (b) 37 years after 1000 MT Supercritical CO_2 Injection into the Ortley Flow Top. Ambient pH is 9.6.

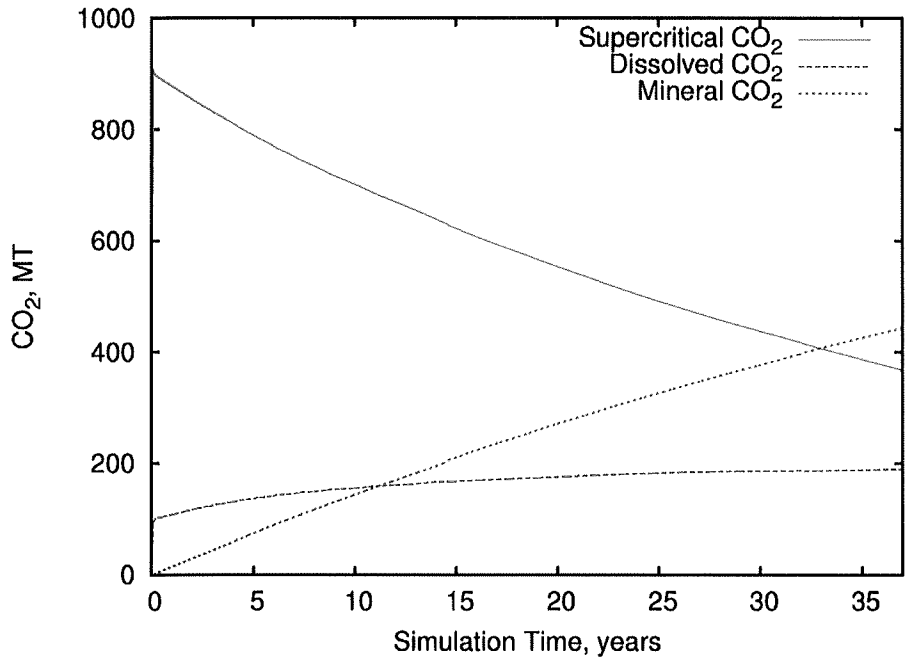

Figure 24. Mass balance of 1000 MT of CO_2 Injection into the Ortley Flow Top.

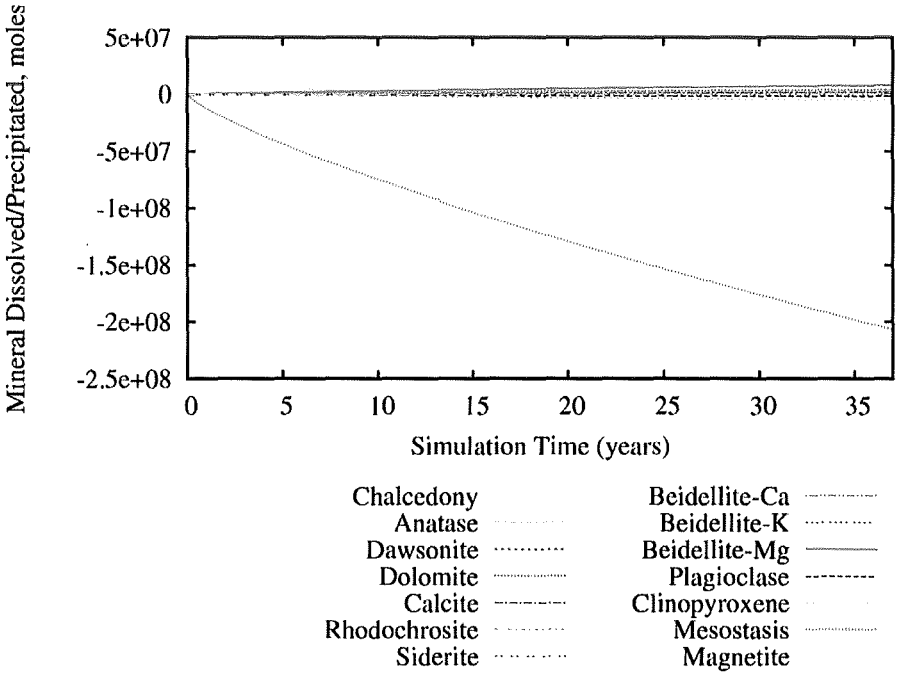

Figure 25. Change in mineral mass (total moles in model domain, negative value indicates dissolution, positive value indicates precipitation) after 1000 MT of CO_2 Injection into the Ortley Flow Top.

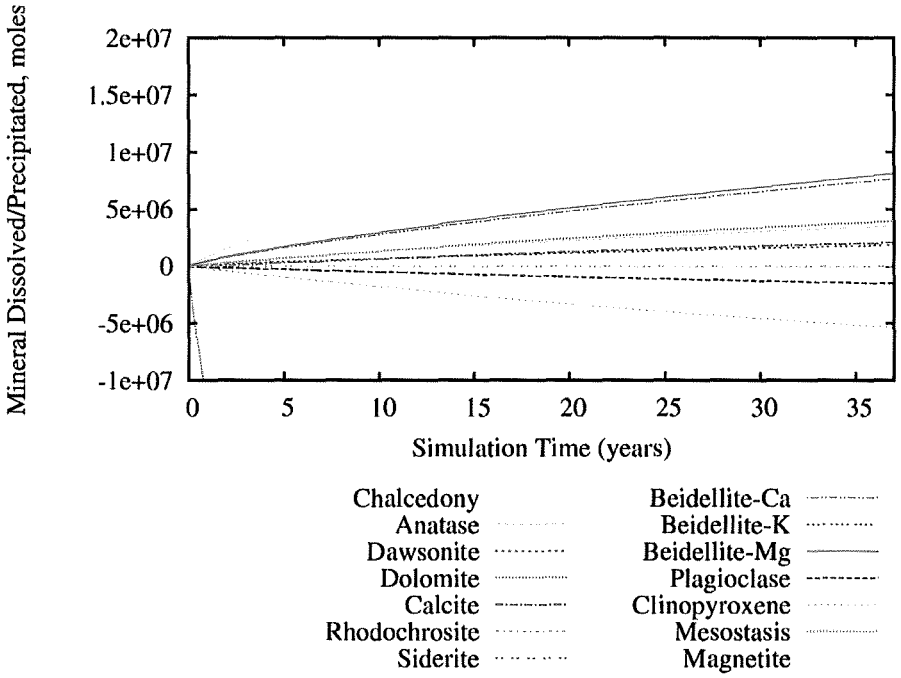

Figure 26. Closeup of Figure 25 showing detail of minerals other than mesostasis (total moles in model domain).

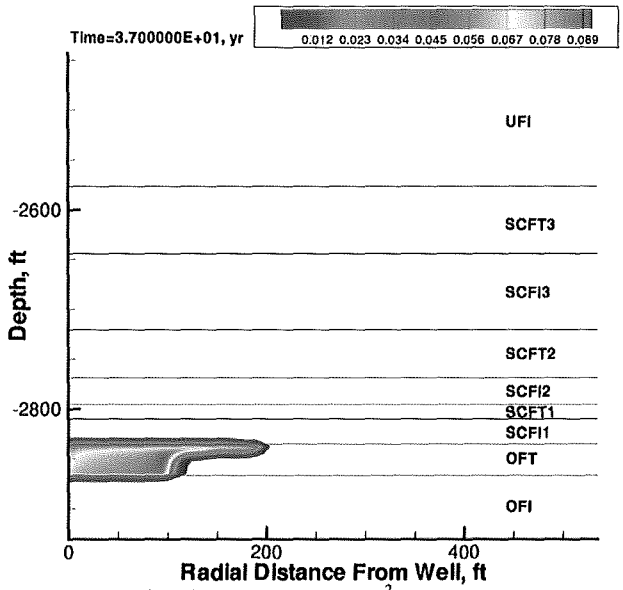

Figure 27. Distribution of precipitated dolomite (moles m^{-3}) 37 years after 1000 MT of CO_2 Injection into the Ortley Flow Top.

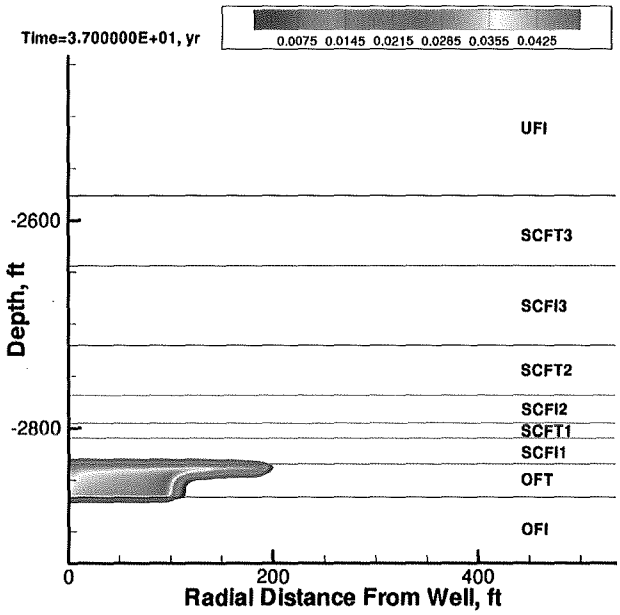

Figure 28. Distribution of precipitated calcite (moles m^{-3}) 37 years after 1000 MT of CO_2 Injection into the Ortley Flow Top.

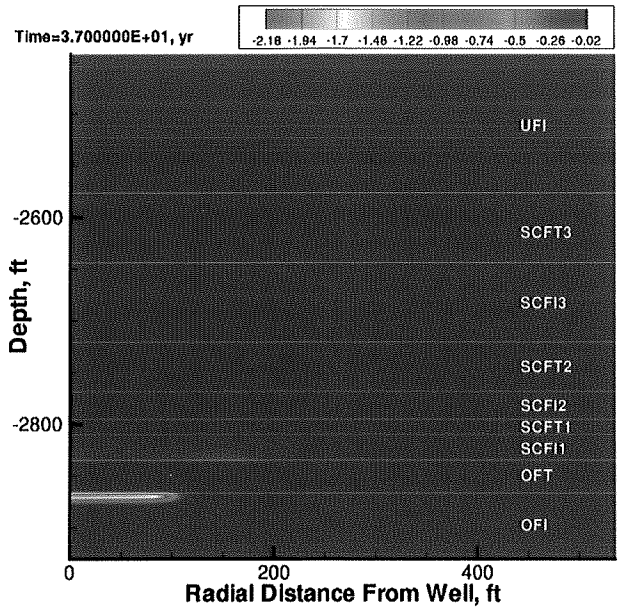

Figure 29. Porosity change (%) in formation 37 years after 1000 MT of CO_2 Injection into the Ortley Flow Top.

The density of the injected supercritical CO_2 is 60% of that exhibited by groundwater at the prevailing formation temperature and pressure conditions. Because supercritical CO_2 does not displace all of the groundwater within the formation pore space, and a significant amount of the supercritical CO_2 has dissolved or precipitated, the average fluid-density contrast is 75% to 100% of that exhibited by the initial formation water after 14 days (Figure 30a) and 90% to 100% that of initial formation water after 37 years (Figure 30b).

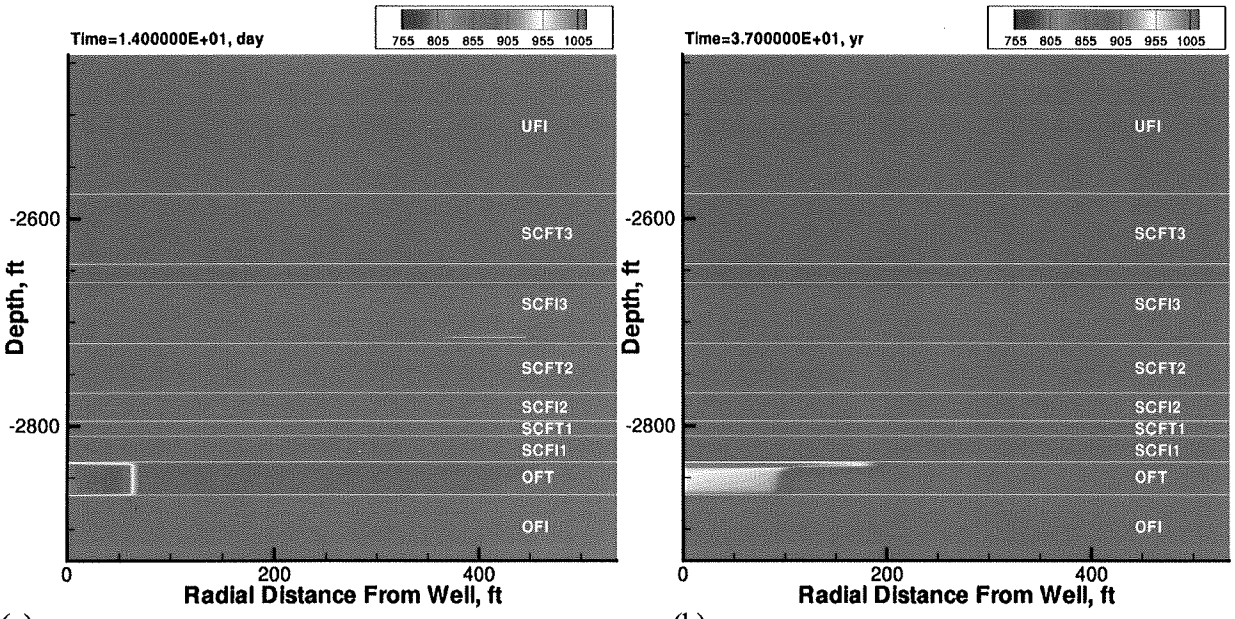

Figure 30. Fluid Density (kg/m^3) in the Ortley Flow Top (a) 14 days and (b) 37 years after start of 1000 MT Supercritical CO_2 Injection

1.3.2 Summary and Conclusions

For 1000 MT of supercritical CO_2 injected into the 3 flow tops (OFT, SCFT1, SCFT2) or the SCFT2 alone, the radii begins to decrease after 13 years. For 1000 MT of supercritical CO_2 injected into the OFT alone, the radii begins to decrease after 37 years. Significant amounts of CO_2 are sequestered both as dissolved CO_2 and in carbonate minerals (Table 6). In all cases, localized changes in formation porosity are low over the time periods considered. The porosity change is lowest in the highest permeability formation, because the injected CO_2 spreads further.

Table 6. Phase distribution of, and porosity change due to 1000 MT of supercritical CO_2 injection once radius has begun to decrease.

Scenario	Time, yr	Target Formation	Injection Duration, days	Supercritical CO_2, %	Dissolved CO_2, %	Mineral CO_2, %	Maximum Porosity Change, %
1	13	SCFT2, SCFT1, OFT	14	50.4%	24.8%	24.8%	1.86
2	13	SCFT2	14	51.0%	24.6%	24.4%	1.15
3	37	OFT	30	36.7%	18.9%	44.3%	2.18

1.3.3 References

McGrail BP, EC Sullivan, PD Thorne, FA Spane, Jr., CJ Thompson, DH Bacon, SP Reidel, G Hund, and FS Colwell. 2009. *Preliminary Hydrogeologic Characterization Results from the Wallula Basalt Pilot Study*. PNWD-4129, Battelle, Pacific Northwest Division, Richland, Washington.

Palandri JL and YK Kharaka. 2004. *A Compilation of Rate Parameters of Water-Mineral Interaction Kinetics for Application to Geochemical Modeling*. U.S. Geological Survey, Menlo Park, California.

Schaef HT, BP McGrail, and AT Owen. In Press. "Carbonate Mineralization of Volcanic Province Basalts." *International Journal of Greenhouse Gas Control.*

White MD and BP McGrail. 2005. *STOMP, Subsurface Transport Over Multiple Phases, Version 1.0, Addendum: ECKEChem, Equilibrium-Conservation-Kinetic Equation Chemistry and Reactive Transport*. PNNL-15482, Pacific Northwest National Laboratory, Richland, Washington.

Wolery TW and RL Jarek. 2003. *Software User's Manual, EQ3/6, Version 8.0*. Sandia National Laboratories, Albuquerque, New Mexico.

Xu TF, JA Apps, and K Pruess. 2005. "Mineral sequestration of carbon dioxide in a sandstone-shale system." *Chemical Geology*, 217:295-318.